


## Article

# Indirect Voltammetry Detection of Non-Electroactive Neurotransmitters Using Glassy Carbon Microelectrodes: The Case of Glutamate

Sandra Lara Galindo <sup>1,2</sup>, Surabhi Nimbalkar <sup>1,2</sup>, Alexis Oyawale <sup>1,2</sup>, James Bunnell <sup>1,2</sup>, Omar Nunez Cuacuas <sup>1,2</sup>, Rhea Montgomery-Walsh <sup>1,2</sup>, Amish Rohatgi <sup>1,2</sup>, Brinda Kodira Cariappa <sup>1,2</sup>, Abhivyakti Gautam <sup>1,2</sup>, Kevin Peguero-Garcia <sup>1,2</sup>, Juyeon Lee <sup>1,2</sup>, Stephanie Ingemann Bisgaard <sup>3</sup>, Carter Faucher <sup>1,2</sup>, Stephan Sylvest Keller <sup>3</sup> and Sam Kassegne <sup>1,2,\*</sup> 

<sup>1</sup> NanoFAB.SDSU Research Lab, Department of Mechanical Engineering, College of Engineering, San Diego State University, 5500 Campanile Drive, San Diego, CA 92182-1323, USA

<sup>2</sup> NSF-ERC Center for Neurotechnology (CNT), San Diego, CA 92182, USA

<sup>3</sup> National Centre for Nano Fabrication and Characterization, DTU Nanolab, Technical University of Denmark, Ørsteds Plads, Building 347, 2800 Kongens Lyngby, Denmark

\* Correspondence: kassegne@sdsu.edu; Tel.: +1-(760)-402-7162

**Abstract:** Glassy carbon (GC) microelectrodes have been successfully used for the detection of electroactive neurotransmitters such as *dopamine* and *serotonin* through voltammetry. However, non-electroactive neurotransmitters such as *glutamate*, *lactate*, and *gamma-aminobutyric acid (GABA)* are inherently unsuitable for detection through voltammetry techniques without functionalizing the surface of the microelectrodes. To this end, we present here the immobilization of the *L-glutamate oxidase (GluOx)* enzyme on the surface of GC microelectrodes to enable the catalysis of a chemical reaction between *L-glutamate*, oxygen, and water to produce H<sub>2</sub>O<sub>2</sub>, an electroactive byproduct that is readily detectable through voltammetry. This immobilization of *GluOx* on the surface of bare GC microelectrodes and the subsequent catalytic reduction in H<sub>2</sub>O<sub>2</sub> through fast-scan cyclic voltammetry (FSCV) helped demonstrate the indirect in vitro detection of *glutamate*, a non-electroactive molecule, at concentrations as low as 10 nM. The functionalized microelectrodes formed part of a four-channel array of microelectrodes (30 μm × 60 μm) on a 1.6 cm long neural probe that was supported on a flexible polymer, with potential for in vivo applications. The types and strengths of the bond between the GC microelectrode surface and its functional groups, on one hand, and *glutamate* and the immobilized functionalization matrix, on the other hand, were investigated through molecular dynamic (MD) modeling and Fourier transform infrared spectroscopy (FTIR). Both MD modeling and FTIR demonstrated the presence of several covalent bonds in the form of C-O (*carbon-oxygen polar covalent bond*), C=O (*carbonyl*), C-H (*alkenyl*), N-H (*hydrogen bond*), C-N (*carbon-nitrogen single bond*), and C≡N (*triple carbon-nitrogen bond*). Further, penetration tests on an agarose hydrogel model confirmed that the probes are mechanically robust, with their penetrating forces being much lower than the fracture force of the probe material.

**Keywords:** glassy carbon; FSCV; glutamate; neurotransmitters; microelectrodes; microfabrication



**Citation:** Galindo, S.L.; Nimbalkar, S.; Oyawale, A.; Bunnell, J.; Cuacuas, O.N.; Montgomery-Walsh, R.; Rohatgi, A.; Cariappa, B.K.; Gautam, A.; Peguero-Garcia, K.; et al. Indirect Voltammetry Detection of Non-Electroactive Neurotransmitters Using Glassy Carbon Microelectrodes: The Case of Glutamate. *C* **2024**, *10*, 68. <https://doi.org/10.3390/c10030068>

Academic Editors: Kunal Mondal, Ankur Gupta and Monsur Islam

Received: 9 May 2024

Revised: 23 July 2024

Accepted: 29 July 2024

Published: 31 July 2024



**Copyright:** © 2024 by the authors. Licensee MDPI, Basel, Switzerland. This article is an open access article distributed under the terms and conditions of the Creative Commons Attribution (CC BY) license (<https://creativecommons.org/licenses/by/4.0/>).

## 1. Introduction

Neurotransmitters play a pivotal role in a large variety of neurophysiological functions [1–4]. For example, *dopamine* (DA) is involved in several neurophysiological processes, such as motor control, reward, motivation, and cognitive function [5–8], whereas *serotonin* (*5-Hydroxytryptamine (5-HT)*) plays a significant role in several neural signal processes, such as memory, long-term potentiation, and cardiovascular and gastrointestinal functions [9–12]. The disruption of the secretion and uptake of DA and 5-HT at synapses is considered a causative factor towards several psychiatric and neurological

disorders [12–15]. Further, 5-HT is a major target for pharmacological treatment, and its involvements in mood disorders and neuroplasticity after injury is of significant research and clinical interest [16]. *Glutamate* and *lactate*, two closely related neurotransmitters, are involved in the metabolic pathways of the central nervous system (CNS), with *glutamate* being the most extensive free-standing amino acid in the brain, with its increased presence identified as a potential cause for significant neuronal cell damage or epileptic seizures [17–22]. Given their significant roles, the understanding of electrochemical neural signaling enabled by neurotransmitters could, therefore, help develop a more complete picture of brain functions and provide a better insight into some key neurological disorders [22–26]. Further, the integration of neurochemical sensing with electrophysiological recording and stimulation is of fundamental importance in elucidating the relationship between electrical and electrochemical signaling and their role in the pathogenesis of neurological disorders [27–29]. This increased understanding could also inform the design of novel closed-loop treatment platforms enabled by neurochemical feedback [30–32]. Therefore, there is a significant research need for developing new electrode technology for the in vivo detection of these neurotransmitters. From a detection point of view, neurotransmitters can be broadly classified into two general groups, i.e., electroactive and non-electroactive. For example, *dopamine*, *serotonin*, and *adenosine* are electroactive species that can electrochemically oxidize, forming *quinone* groups [33–37]. Techniques such as fast-scan cyclic voltammetry (FSCV) can then be used for the direct detection of such electroactive species through their respective signature redox peaks. On the other hand, neurotransmitters such as *glutamate*, *lactate*, *acetylcholine*, and *gamma-aminobutyric acid (GABA)* are non-electroactive and are, therefore, inherently unsuitable for direct detection through voltammetry techniques. For this and several other reasons, such as no requirement for specialized equipment and post-processing of data, most works reported in the literature in the detection of such non-electroactive neurotransmitters had used amperometric techniques [38,39]. However, the major drawback of amperometric techniques are their non-selectivity and relatively slow response time, which—in the context of simultaneous detection of multiple neurotransmitters—make them impractical for such needs. This has given rise to the exploration of FSCV for the detection of *glutamate* along with other neurotransmitters, such as *dopamine*. FSCV has emerged as a method of choice for in vivo applications due to its sub-second scale temporal resolution that is in the same time scale as synaptic chemical fluctuations [40]. Using FSCV, a recent work had demonstrated the indirect detection of *glutamate* through *GlutOx-chitosan* hydrogels electrodeposited on carbon-fiber microelectrodes (CFMs) [41]. However, carbon-fiber microelectrodes have their own shortcomings, such as lack of mechanical sturdiness, inconsistent composition, and surface adsorption properties, which have in turn limited their repeatability and reliability [42].

To address these gaps, recent works have introduced a lithographically patternable array of carbon-based microelectrodes that have shown promises in neurotransmitter detections. Among these, glassy carbon (GC) has emerged as a compelling material of choice for microelectrodes used in the detection of electroactive neurotransmitters, such as *DA* and *5-HT*, at concentrations as low as 10 nM [43–48]. Further, due to its surface that is rich with electrochemically active functional groups, good adsorption characteristics, and its antifouling properties, GC has been demonstrated to be useful for not only electrophysiological recordings and stimulations but also for the multi-site simultaneous detection of electroactive neurotransmitters, *DA* and *5-HT*, in a stable and repeatable manner [47,48]. However, for the indirect detection of non-electroactive neurotransmitters, such as *glutamate*, *lactate*, and the like, surface functionalization of microelectrodes is required. One such possibility is the immobilization of the *glutamate oxidase (GluOx)* enzyme on the surface of microelectrodes to enable the catalysis of the chemical reaction between *L-glutamate*, oxygen, and water to produce the electroactive byproduct *hydrogen peroxide*, which is detectable through voltammetry ( $L\text{-glutamate} + \text{oxygen} + \text{water} \rightarrow \text{oxoglutarate} + \text{ammonia} + \text{hydrogen peroxide}$ ). In lieu of *GluOx*, *glutamate dehydrogenase* could also be used for the detection of *glutamate* [49–51]. In this study, we extend the application of GC

to the detection of non-electroactive neurotransmitters and present the immobilization of *GluOx* on lithographically patterned GC microelectrodes for establishing the indirect electrochemical in vitro detection of *glutamate*. The same platform could be used for the detection of other neurotransmitters through an appropriate surface functionalization.

## 2. Materials and Methods

### 2.1. Microfabrication of Microelectrodes

A 1.6 cm long penetrating neural probe with four GC microelectrodes of  $30\ \mu\text{m} \times 60\ \mu\text{m}$  size was microfabricated. As described elsewhere, the microfabrication process for the probe shown in Figure 1a involved spin coating of SU-8 negative photoresist (Microchem, Boston, MA, USA) on a silicon wafer (with  $0.5\ \mu\text{m}$  thick oxide layer) at 1200 rpm for 55 s and soft baking at  $65\ ^\circ\text{C}$  for 10 min and  $95\ ^\circ\text{C}$  for 20 min, followed by UV exposure at  $\sim 400\ \text{mJ}/\text{cm}^2$  [52]. This was followed by a post-exposure bake at  $65\ ^\circ\text{C}$  for 1 min and  $95\ ^\circ\text{C}$  for 5 min, development of SU-8 for 3–5 min, and curing at  $150\ ^\circ\text{C}$  for 30 min. Pyrolysis was carried out at  $1000\ ^\circ\text{C}$  in an inert  $\text{N}_2$  environment following protocols described elsewhere [52–54]. Subsequently,  $5\ \mu\text{m}$  layer of photo-patternable polyimide (HD 4100) (HD Microsystems, Wilmington, DE, USA) was spin-coated on top of the GC microelectrodes at 2500 rpm for 45 s, soft-baked at  $90\ ^\circ\text{C}$  for 3 min and at  $120\ ^\circ\text{C}$  for 3 min, then cooled down to room temperature, and patterned through UV exposure at  $\sim 400\ \text{mJ}/\text{cm}^2$ . Then, the polyimide layer was partially cured at  $300\ ^\circ\text{C}$  for 60 min under  $\text{N}_2$  environment. Following, Pt metal traces with Ti adhesion layer were patterned using a metal lift-off process. For electrical insulation, an additional  $6\ \mu\text{m}$  of polyimide HD 4100 was spin-coated (300 rpm), patterned ( $400\ \text{mJ}/\text{cm}^2$ ), and cured ( $350\ ^\circ\text{C}$  for 90 min) under  $\text{N}_2$  environment. An additional  $30\ \mu\text{m}$  thick layer of polyimide (Durimide 7520, Fuji Film, Tokyo, Japan) was spin-coated (800 rpm, 45 s) and then patterned ( $400\ \text{mJ}/\text{cm}^2$ ) on top of the insulation layer to reinforce the penetrating portion of the device (Figure 1b). Once the probes were released from the carrier substrate using a BHF bath, the GC microelectrodes were plasma-etched (120 W for 45 s) and then functionalized through drop casting of an enzyme mix's thin coat.

### 2.2. Functionalization of Microelectrodes

As shown in Figure 1c, the surface functionalization process consisted of preparing an enzyme immobilization matrix made of *glutamate oxidase* (*GluOx*), a catalytic enzyme, *glutaraldehyde* (a reagent from the aldehyde family that allows a rapid ionic immobilization of the enzyme on the GC microelectrode surface), and *bovine serum albumin* (*BSA*) which provides stability to the enzyme and the reagent mixture. *L-glutamic acid* ( $\geq 99\%$ ), *L-glutamate oxidase* (from *Streptomyces* sp.), and *bovine serum albumin* ( $\geq 96\%$ ) were purchased from Sigma Aldrich (St. Louis, MO, USA). In addition, *glutaraldehyde* (25% solution distillation purified) was purchased from Electron Microscopy Sciences (Hatfield, PA, USA). Before mixing, *GluOx*, *glutaraldehyde*, and *BSA* were brought to room temperature. Then, the *GluOx* enzyme was dissolved in  $1\ \mu\text{L}$  of DI water. Separately,  $0.01\ \text{g}$  of *BSA* was placed in a microcentrifuge tube and  $985\ \mu\text{L}$  of DI water was added to it. The mix was then vortexed at low rpm. Subsequently,  $5\ \mu\text{L}$  of *glutaraldehyde* was added. This mixture of *BSA/glutaraldehyde* was then transferred into a  $500\ \mu\text{L}$  microcentrifuge tube,  $1\ \mu\text{L}$  of *GluOx* was added to it, and it was vortexed again at slow rpm. This was followed by dry storage of the immobilization matrix at room temperature to ensure a successful crosslinking between the enzyme, *glutaraldehyde*, and *BSA*. Finally,  $10\ \mu\text{L}$  of the immobilization matrix was then extracted and pipetted for drop casting of a thin coat over the surface of the GC microelectrodes.

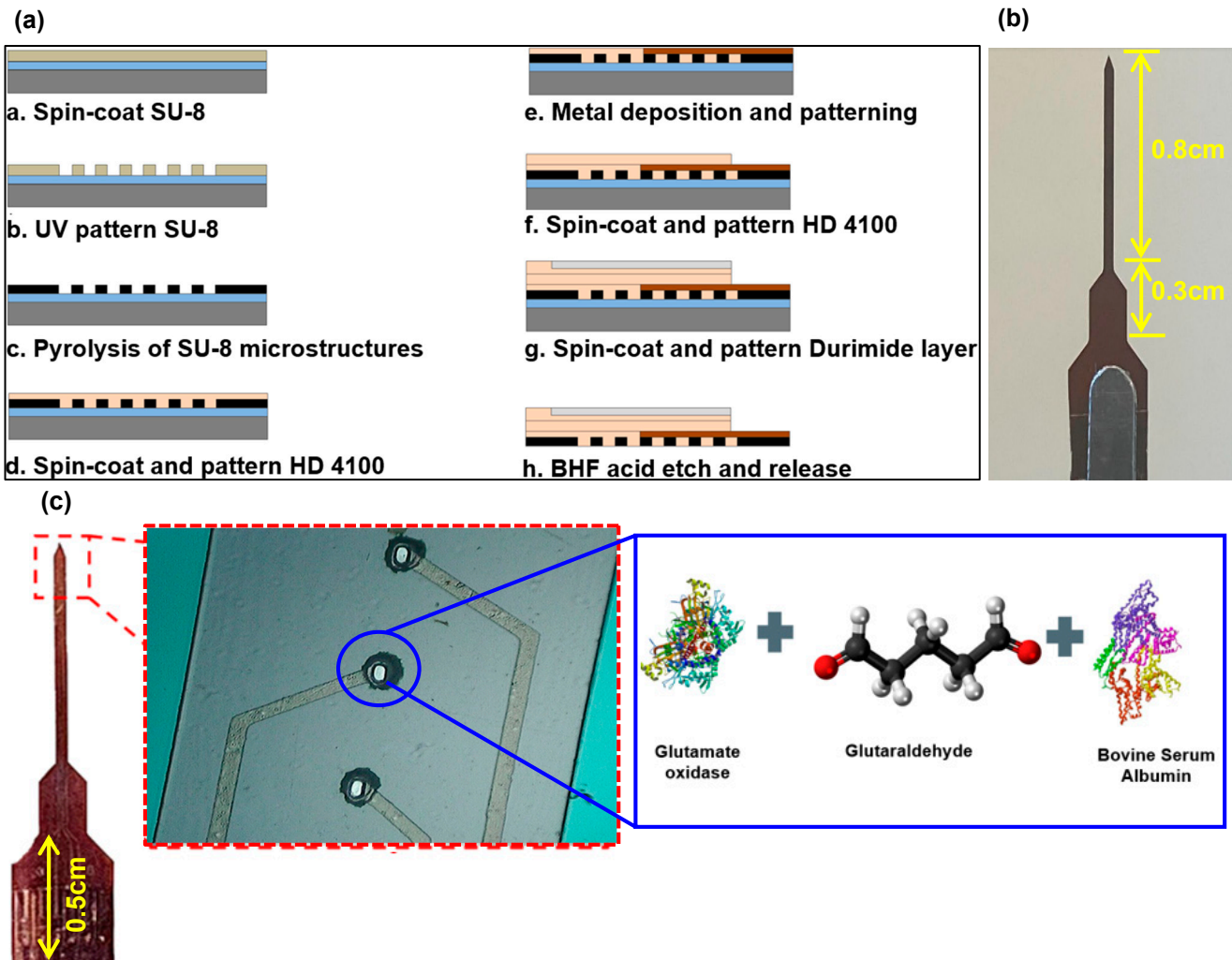


**Figure 1.** (a) Microfabrication steps for 4-channel penetrating neural probes (1.6 cm long) mounted on polymeric substrate; (b) fabricated probe for neurotransmitter detection application; (c) GC microelectrodes of  $30\ \mu\text{m} \times 60\ \mu\text{m}$  size and  $140\ \mu\text{m}$  spacing coated with the *GluOx*, *glutaraldehyde*, and *BSA* mixture.

### 2.3. Mechanical Characterization

The mechanical stability of the probes and their penetration ability were tested using a TA.XT plusC Texture Analyzer (TA) (Stable Micro Systems Products, Hamilton, MA, USA). To determine an appropriate agarose gel concentration that models the modulus of brain tissue, a compression calibration test was first carried out as explained in the accompanying Supplementary Document (Section S1) [55–58]. Once the relevant concentration of agarose gel was determined, penetration tests of the *in vitro* model medium were carried out using the GC probes presented in Figure 1. For this, a holder for the GC probe was designed, 3D-printed, and mounted on the probe of the TA (Figure 2). The agarose gel block shown in Figure 2 had a length of 30 mm, width of 30 mm, thickness of 10 mm, and area of  $900\ \text{mm}^2$ . The same speed of loading of 2 mm/s was used for the penetration test as well, with a 0.5 kg weight load cell.

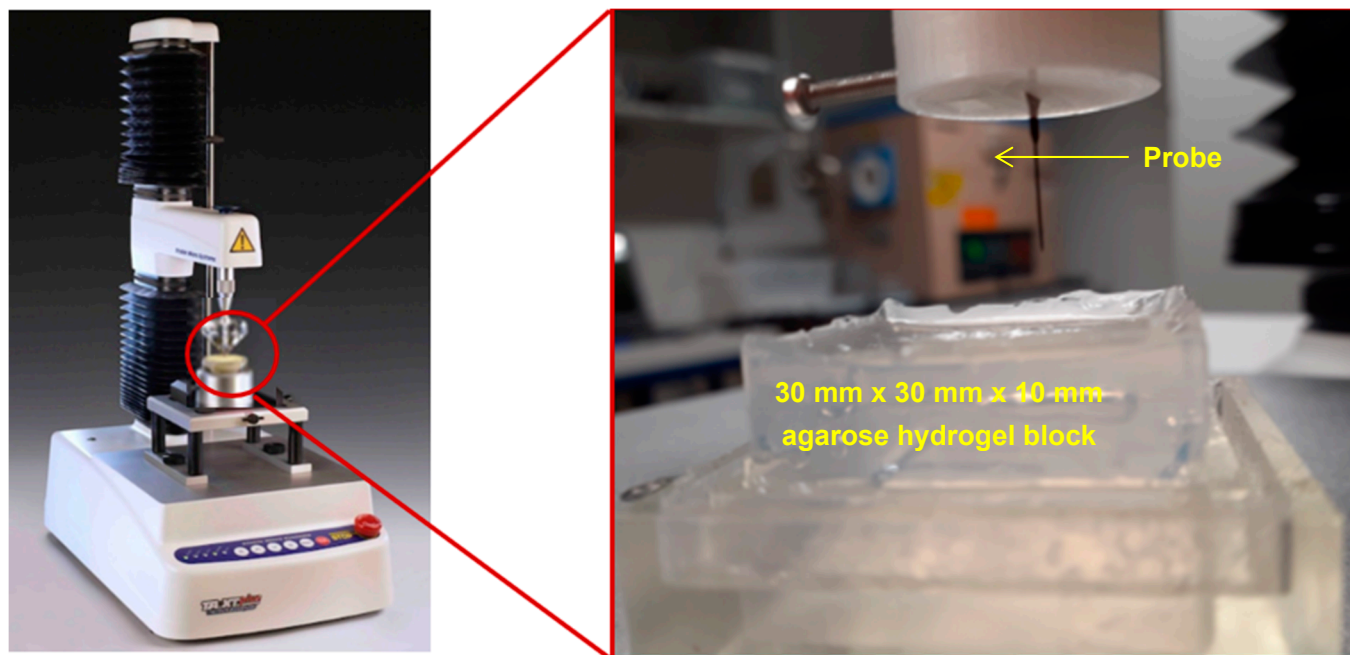


**Figure 2.** TA.XT plusC Texture Analyzer holding a probe for penetration tests.

#### 2.4. Molecular Dynamic (MD) Modeling

To explore the interaction between *glutamate* and the immobilized enzyme mix with the surface of GC microelectrodes and investigate if covalent bonds were formed, a chemical simulation was performed using molecular dynamic (MD) modeling software. We used ReaxFF software from SCM-ReaxFF (AMS2023), a tool for modeling chemical reactions with a reactive force field [59]. Briefly, in this reactive force field formulation of ReaxFF, a pre-determined potential energy function allows for the calculation of the force experienced by any atom, given the positions of all its surrounding atoms at a given time step. The forces acting on each atom at each time step are computed using molecular mechanic force fields. The position and velocity of each atom and energy contributions to the potential are then updated using Newton's equations of motion. The total force consists of the energy associated with forming bonds between atoms, the valence angle strain and torsional angle strain, and electrostatic and dispersive contributions between all atoms. The starting model of the molecular structure of GC was the nanostructure that was reported in our recent work, which consisted of a flat graphitic domain with graphene-like 6-membered carbon rings and a cage-like component [60]. For simplicity, the simulation cell used here ( $25 \text{ \AA} \times 25 \text{ \AA} \times 25 \text{ \AA}$ ) with a density of  $1.19 \text{ g/mL}$  modeled only the flat component consisting of 144 graphene-like 6-membered carbon rings, as shown in Figure 3. Four functional groups (*carbonyl*, *carboxyl*, *hydroxyl*, and *epoxy*) were considered to be attached to this carbon molecule. The 5- and 7-membered carbon rings that form the periphery of the cagey component along with 6-membered carbon rings were expected to have similar chemical interactions and were not included in the model to save computational expenses.

With regard to modeling *GluOx*, which is a relatively large protein structure, the required significantly high computational resources could be a limiting factor. However, since all proteins and amino acids contain both C- and N-terminal domains, the amino acid *glutamate* can be taken as a smaller representation of the large molecule of *GluOx*, thereby achieving a more efficient way of predicting chemical interactions between the key amino acid components and the carbon surface. This is further supported by the fact that *glutamate* is one of seven amino acids present in the active site of *GluOx*, suggesting that it plays an essential role in the production of  $\text{H}_2\text{O}_2$ . A full list of key amino acids that are present in the active site, along with their functional groups, are given in Table S1 for completeness. With this reasoning, the *glutamate* ( $\text{C}_5\text{H}_9\text{NO}_4$ ) molecule was added to the simulation cell.

Two temperature cases (27 °C and 37 °C) and two voltage bias cases (0 V and 0.4 V) were considered. All models were analyzed using a temperature damping constant of 100 fs and a pressure damping constant of 500 fs with constant volume and temperature conditions through the constant temperature and volume (NVT) Berendsen thermostat [61,62].

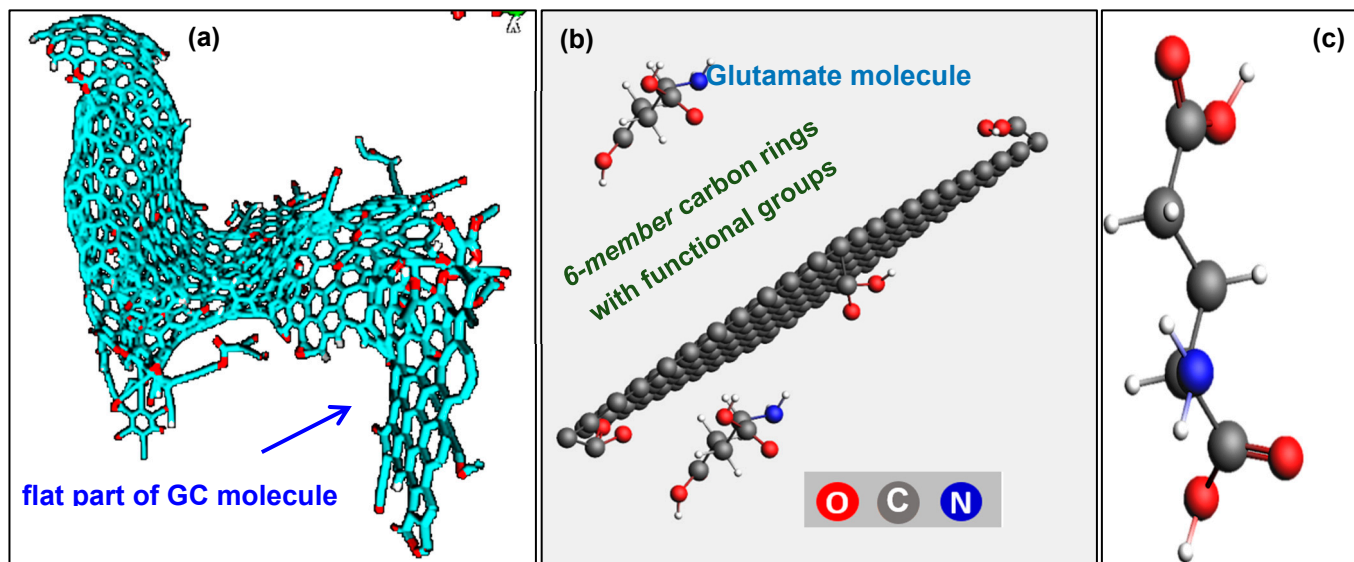


**Figure 3.** (a) GC molecule [58]; (b) MD model consisting of only 6-membered carbon rings with functional groups (carbonyl, carboxyl, hydroxyl, and epoxy) and glutamate molecules in a simulation cell of 25 Å × 25 Å × 25 Å; (c) single glutamate (C<sub>5</sub>H<sub>9</sub>NO<sub>4</sub>) molecule which is considered to represent an active site of *GluOx* in this study.

### 2.5. FTIR Spectroscopy

To determine the presence of functional groups and, by correlation, the strength of the bond between the GC microelectrode surface and the immobilized functionalization mix, FTIR-ATR spectroscopy was carried out using a Nicolet iS50 FTIR Spectrometer equipped with a Smart iTR diamond ATR cell (Thermo Scientific, Court Vernon Hills, IL, USA). Three types of samples were analyzed: a bare GC microelectrode that was used as control, a plasma-etched GC microelectrode (120 W for 45 s) with a coating of *GluOx* mixture containing glutaraldehyde and BSA, and a GC microelectrode with a *GluOx* mixture without glutaraldehyde and BSA. Each sample was washed with methanol, dried, and placed on diamond cell, followed by recordings of 128 spectral scans that were subsequently compiled from 4 diagonal areas of the microelectrodes.

### 2.6. Voltammetry

Indirect detection of glutamate through direct electrochemical detection of the conversion product H<sub>2</sub>O<sub>2</sub> was performed with a WaveNeuro Potentiostat System (Pine Research, Durham, NC, USA). The surface functionalized GC microelectrode was used as the working electrode with a standard Ag/AgCl reference electrode. The electrolyte solution was phosphate-buffered saline (PBS) (0.01 M, pH 7.4; Sigma Aldrich, St. Louis, MO, USA). A waveform consisting of triangle scan at scan rate of 400 V/s from −0.5 V to +1.3 V with a holding potential of −0.5 V with respect to Ag/AgCl reference electrode was used. The duration of each scan was 9 ms with 10 Hz frequency. The same voltage waveform was applied to microelectrodes at 60 Hz for 1 h prior to the start of each experiment for pre-conditioning. Known concentrations of glutamate (10 nM–1.6 μM) were then infused over 5 s, while changes in current were recorded for 30 s. For a control experiment, a separate probe with no surface functionalization was subjected to the same waveform. Data analysis and background-subtracted cyclic voltammograms (CVs) were performed using HDCV software (Electronics Facility, Chapel Hill, NC, USA).

### 3. Results and Discussion

#### 3.1. Mechanical Characterization

Figure 4 shows the force–displacement plots for the penetration force test of the neural probe for the agarose hydrogel of a 0.6% concentration, which was found to be a good model for brain tissue (Section S2). The first clearly identifiable peak shown in Figure 4 corresponds to the first section of the neural probe penetrating the surface of the gel. The penetration force is then identified as the first maximum of the force–displacement curve. The force needed to penetrate the 0.6% agarose hydrogel simulating the brain tissue was  $0.0035 \pm 0.00015$  N ( $n = 5$ ); for the 1.5% agarose hydrogel, the penetration force was  $0.0051 \pm 0.00028$  N ( $n = 4$ ).

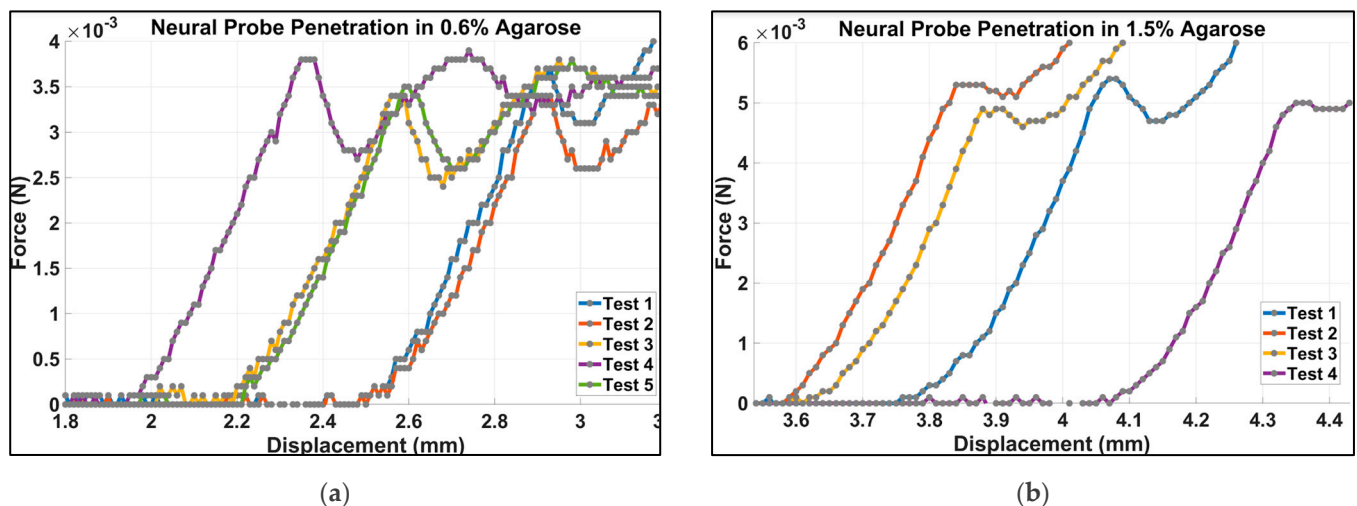


**Figure 4.** Penetration force measurements for (a) 0.6% and (b) 1.5% agarose gel concentrations.

#### 3.2. Molecular Dynamic Modeling

We explored the interaction of the functional groups ( $\text{COOH}$ ,  $\text{CO}$ ,  $\text{OH}$ , and  $\text{O}$ ) on the carbon microelectrode material with *glutamate* and the immobilized enzyme mix. For this, we considered the effect of electrical bias (0 V, 0.4 V), temperature (25 °C and 37 °C), type of functional groups, number of molecules of *glutamate*, and the lattice of the 6-member carbon ring group on this interaction. Several potential interactions with functional groups to produce covalent bonds were explored. As shown in Figure 5a, the *carboxyl* ( $\text{COOH}$ ) functional group was observed to interact with *glutamate* at a temperature of 25 °C with no electrical bias, with the *glutamate* molecule forming a carbon–oxygen (C–O) covalent bond with the functionalized GC microelectrode surface. This interaction occurred due to the donation of electrons by *glutamate*. The epoxide group was observed to facilitate the formation of a strong carbon–nitrogen (C–N) covalent bond between the nitrogen molecule from *glutamate* and the carbon molecule of the microelectrode (Figure 5b). However, at this temperature and 0 voltage bias, no interactions were observed for the *carbonyl* ( $\text{CO}$ ) and *hydroxyl* ( $\text{OH}$ ) functional groups. Considering a slightly higher temperature of 37 °C, the carbonyl functional group ( $\text{CO}$ ) resulted in a C=O covalent bond (Figure 5c).

In the next set of simulations, the effect of electrical bias was explored under temperatures of 27 °C and 37 °C. In the case of a 25 °C temperature, similar outcomes as the 0 V bias case were observed (Figure 5d,e). However, at a temperature of 37 °C, all the four functional groups were observed to enable the formation of a covalent bond between *glutamate* and the carbon microelectrode’s surface. In the case of the carboxyl group, increasing the temperature to 37 °C combined with electrical bias at 0.4 V resulted in a carbon–nitrogen (C–N) bond (Figure 5f). Similarly, for the carbonyl group, increasing the temperature to 37 °C led to a carbon–nitrogen (C–N) bond, as shown in Figure 5g, demonstrating the effect of an elevated temperature on bond formation. For the hydroxyl group, a carbon–nitrogen (C–N) bond was observed, while in the case of the epoxide group,

an immediate attachment of *glutamate* through a carbon–oxygen (C–O) bond was observed. A summary of the interactions is presented in Table 1.

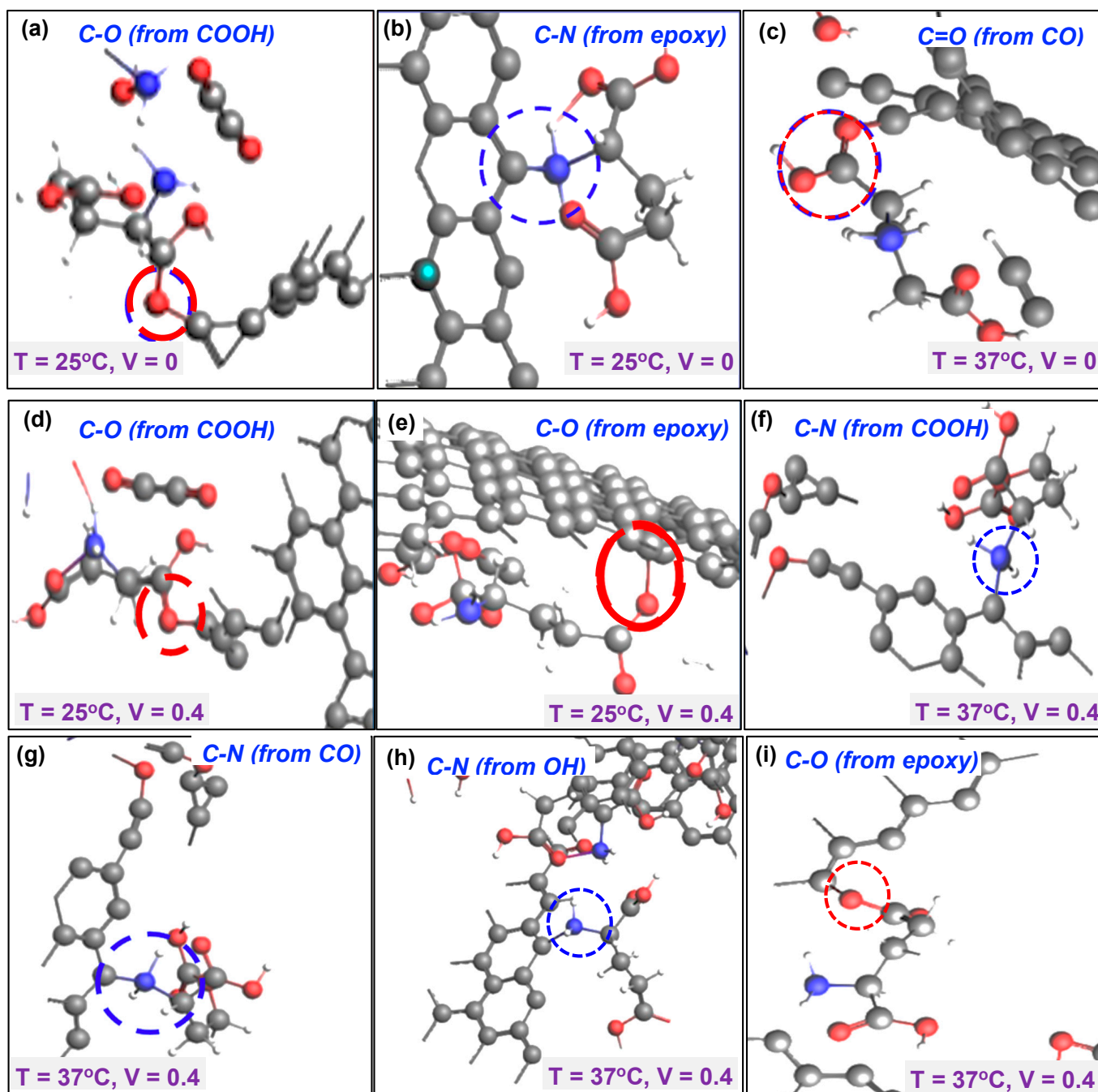


**Figure 5.** (a) C–O bond due to COOH group at 25 °C and no bias; (b) C–O bond due to epoxy group at 25 °C and no bias; (c) C=O bond due to carbonyl group at 37 °C and no bias; (d) C–O bond due to COOH group at 0.4 V and 25 °C; (e) C–O bond due to epoxy at 0.4 V and 25 °C; (f) C–N bond due to COOH group at 0.4 V and 37 °C; (g) C–N bond due to CO group at 0.4 V and 37 °C; (h) C–N bond due to OH group at 0.4 V and 37 °C; (i) C–O bond due to epoxy at 0.4 V and 37 °C.



**Table 1.** Summary of the interaction of the four functional groups on the carbon electrode's surface with enzyme mix and glutamate. Simulation cell of 25 Å × 25 Å × 25 Å was considered with sphere radius of 2 Å.

Voltage/Bias (V)	Temp. (°C)	Functional Group	Outcome	Figure
0	25	COOH (carboxyl)	C-O bond	Figure 5a
		CO (carbonyl)	No bond	
		OH (hydroxyl)	No bond	
		O (epoxy)	C-N bond	Figure 5b
	37	COOH (carboxyl)	No bond	
		CO (carbonyl)	C=O	Figure 5c
		OH (hydroxyl)	No bond	
		O (epoxy)	No bond	
0.4	25	COOH (carboxyl)	C-O bond	Figure 5d
		CO (carbonyl)	No bond	
		OH (hydroxyl)	No bond	
		O (epoxy)	C-O bond	Figure 5e
	37	COOH (carboxyl)	C-N bond	Figure 5f
		CO (carbonyl)	C-N bond	Figure 5g
		OH (hydroxyl)	C-N bond	Figure 5h
		O (epoxy)	C-O bond	Figure 5i

### 3.3. FTIR Characterization

For the bare GC control specimen (inset in Figure 6a), three clear and distinct peaks that ranged between 1435.67 cm<sup>-1</sup> and 755.53 cm<sup>-1</sup> were detected, representing a C-O stretch with a single bond [63]. The second sample had its bare GC surface plasma-etched at 120 W for 45 s before coating it with the *glutamate oxidase* mixture. Figure 6a summarizes several peaks for the *glutamate oxidase* sample on top of GC: the first peak at 3488.55 cm<sup>-1</sup> corresponds to the amine stretch (N-H) that potentially originated from unreacted amino groups in *glutamate oxidase* and *L-glutamate* [64], while the peak at 3071.12 cm<sup>-1</sup> corresponds to the alkenyl (C-H) stretch and its neighbor peak of 3000 cm<sup>-1</sup> corresponds to unsaturated alkene (C=C) compounds. Carboxylic acid (C=O) peaks are represented by a stretch in the region of 1775.28 cm<sup>-1</sup>–719.52 cm<sup>-1</sup> while (C-H) bending vibration with single or multiple absorption bands is represented by 719.52 cm<sup>-1</sup> [65]. For the third sample that was coated with *glutamate oxidase*, more peaks were detected, as shown in Figure 6b, where the characteristic absorption ranged between 2136.93 cm<sup>-1</sup> and 534.48 cm<sup>-1</sup>. The highest fingerprint was 2136.9 cm<sup>-1</sup>, which is a triple bond between the carbon and nitrogen stretch (C≡N), and the second peak was 1753.04 cm<sup>-1</sup>, which corresponds to an aldehyde C=O stretch; this one, in particular, was derived from the *glutaraldehyde* present on the surface of the microelectrode from the enzyme mixture [66].

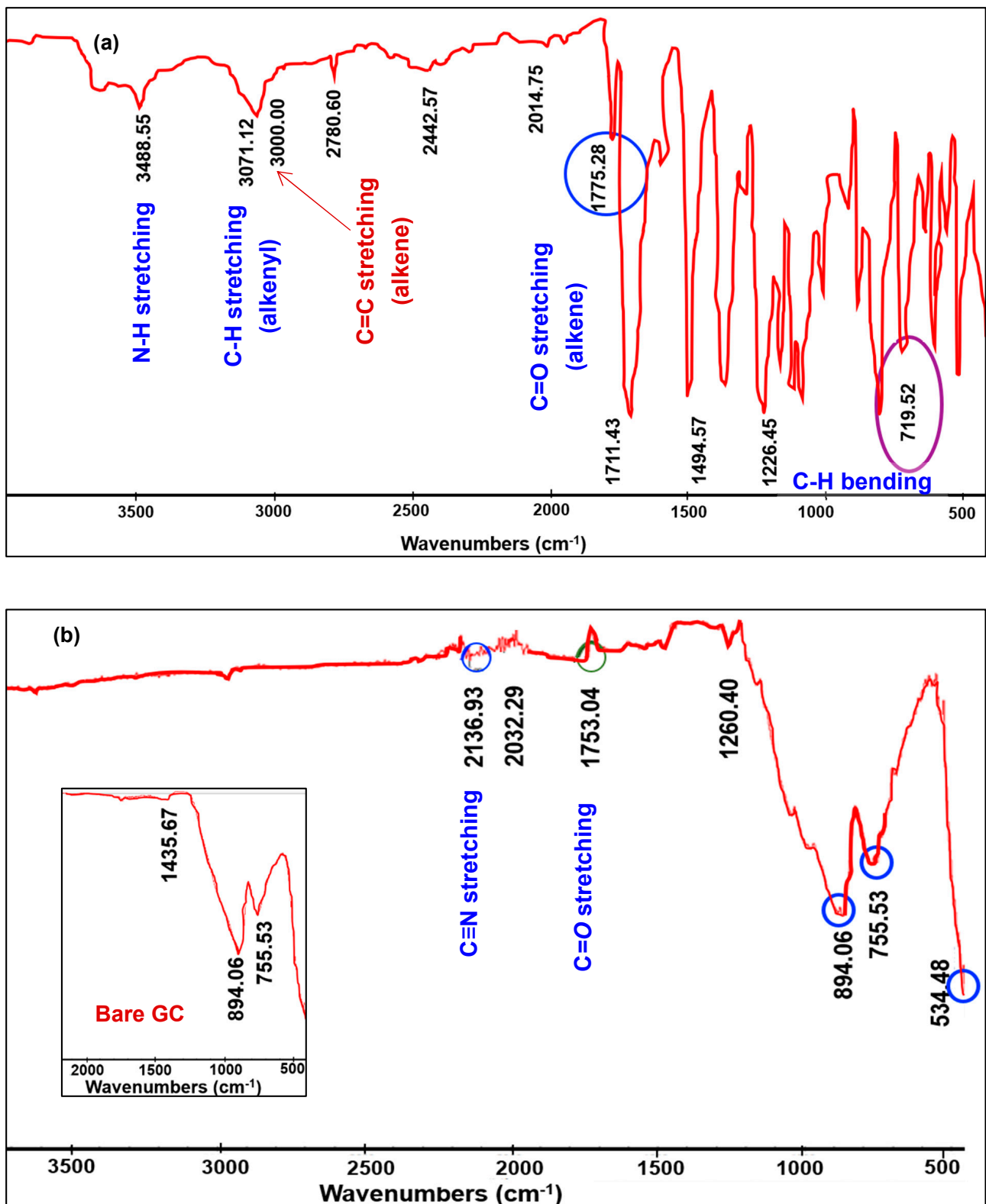


**Figure 6.** (a) FTIR spectra for plasma-etched GC electrode coated with glutamate enzyme (*GluOx* mixture containing glutaraldehyde and BSA); (b) spectra for glutamate oxidase analyzed on top of GC electrode surface. Inset shows the FTIR for bare GC.

### 3.4. In Vitro Glutamate Detection through Voltammetry

As described earlier, due to the non-electroactive nature of *glutamate*, background-subtracted FSCV for *glutamate* was performed indirectly through the immobilization of the *glutamate oxidase* (*GluOx*) enzyme on the surface of GC microelectrodes. The *GluOx* enzyme enabled the catalysis of a chemical reaction between *L-glutamate*, oxygen, and water to produce an electroactive byproduct ( $H_2O_2$ ), which is readily detectable through voltammetry. Since typical FSCV runs result in accelerated oxidation and reduction in analytes on the electrode's surface and hence form an electrical double layer, the background currents (BCs) were subtracted before the peaks could be identified [48]. As a control, the first set of experiments involved injecting a solution of  $H_2O_2$  on a bare GC microelectrode at varying concentrations over a period of 25 min (Table S2). Figure 7a shows the resulting redox peaks in a background-subtracted FSCV for  $H_2O_2$ , with oxidation occurring at 1.2 V and a reduction at  $-0.2$  V [67]. As the second set of control experiment, FSCV was carried out on bare GC electrodes where *glutamate* of varying concentrations was injected. However, there was no redox peaks observed for this control experiment. On the other hand, for the actual experiment, another probe was used where *glutamate* of varying concentrations (10 nM–1.6  $\mu$ M) was injected into the PBS solution. This was performed over a period of 30 min, as shown in Table S2, with sufficient time provided in-between each step to allow for the stabilization of FSCV data collection. Figure 7b shows the resulting background-subtracted FSCV plots, indicating that the GC microelectrode was able to detect the *glutamate conversion* byproduct  $H_2O_2$  obtained at a *glutamate* concentration as low as 10 nM with an oxidation peak at 1.2 V and reduction peak at 0.2 V. False-color plot of Figure 8a shows the transient oxidation and reduction of 200 nM in  $H_2O_2$  injected to the PBS solution (control), while the false-color plot of Figure 8b shows the same for an injection of 10 nM of *glutamate* into the PBS solution.

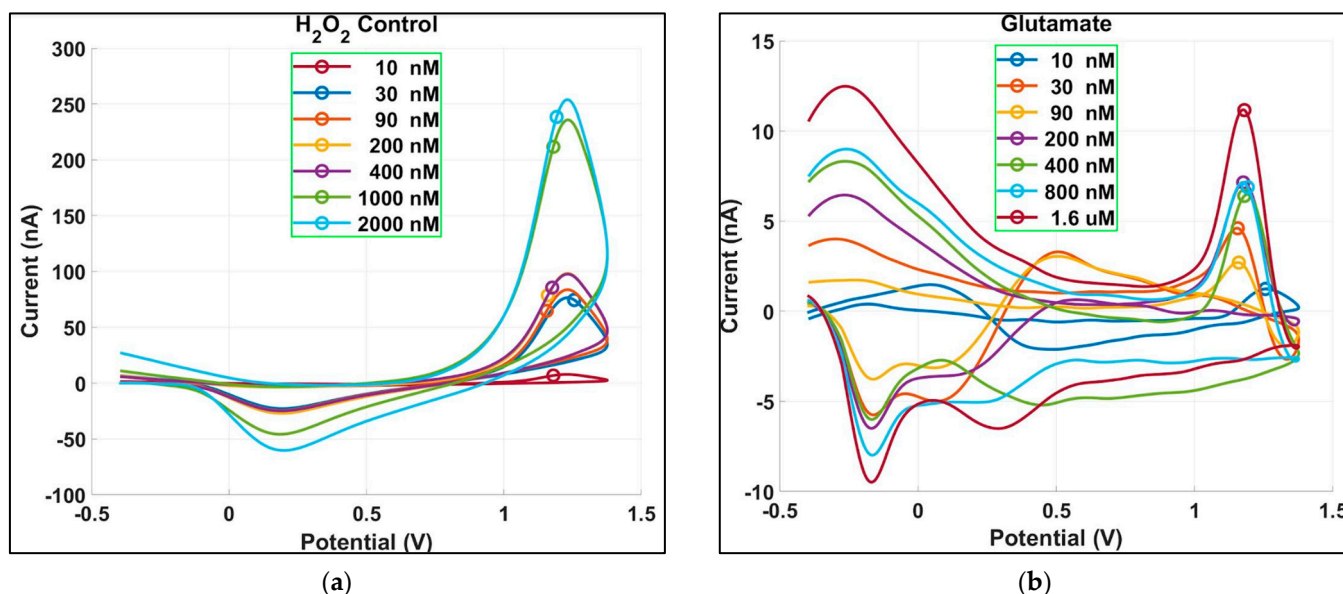


**Figure 7.** (a) Redox peaks in FSCV for detection of  $H_2O_2$  of varying concentrations used as control experiment (10 nM–2  $\mu$ M). (b) Redox peaks in FSCV during indirect *glutamate* detection for 10 nM–1.6  $\mu$ M concentrations.

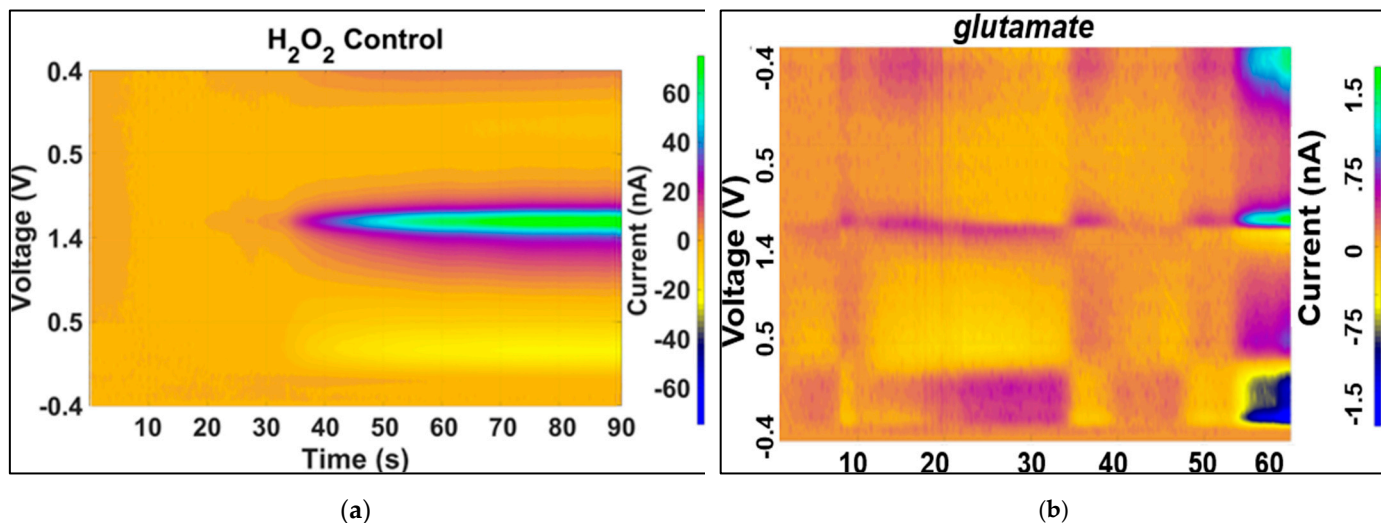


**Figure 8.** (a) Two-dimensional false-color plot corresponding to addition of 200 nM concentration of  $H_2O_2$ ; (b) two-dimensional false-color plot corresponding to addition of 10 nM concentration of *glutamate* to PBS solution.

#### 4. Discussions and Conclusions

While GC was demonstrated to be effective in detecting electroactive neurotransmitters such as *dopamine* and *serotonin* at concentrations as low as 10 nM, its potential use for non-electroactive ones like *glutamate* has so far been unexplored. Against a background of a long-term research interest in the simultaneous detection of multiple neurotransmitters using GC voltammetry electrodes located on the same probe, the extension of this capability of GC to such detection of non-electroactive analytes like *glutamate* carries potential for being able to significantly contribute in the broader research discipline of neurochemistry. In this regard, the first obstacle that had to be addressed in extending its capability to *glutamate* was the integrity of the needed surface functionalization. Two approaches were sought to demonstrate the formation of covalent bonds between the carbon surface and the enzymes used for surface functionalization, i.e., FTIR and reactive molecular dynamic (MD) modeling. FTIR confirmed the existence of a C-O stretch with a single bond, an aldehyde/carboxylic/carbonyl C=O stretch, alkenyl C-H bending, a triple bond between a nitrogen and carbon stretch ( $C\equiv N$ ), and an amine stretch (N-H) that potentially originated from unreacted amino groups in *glutamate oxidase* and *L-glutamate*. On the other hand, MD modeling predicted that C-O and C=O bonds would arise due to *carboxyl* (COOH) and *epoxy* (O) functional groups at 25 °C and 37 °C and predicted no bias conditions. However, in the presence of a nominal voltage bias of 0.4 V and temperature of 37 °C, *carboxyl*, *carbonyl* (CO), and *hydroxyl* (OH) groups were observed to interact with *glutamate*, forming a C-N bond. The absence of an amine stretch (N-H) in the MD simulation could be explained by the absence of unreacted amino groups in the model.

In general, these results obtained through reactive MD modeling regarding bond formations are consistent with what was recently reported in a simulation work regarding the binding properties of pristine graphene and graphene derivatives with *glutamate*, where the bond formations were driven mainly by the same four functional groups, i.e., *COOH*, *carbonyl*, *hydroxyl*, and *epoxy* [68]. Further, simulations based on molecular docking mechanisms between the functional groups and carbon (in the form of graphene) also demonstrated that the *COOH* functional group presented the highest stability among the four groups considered. The observation reported here where all functional groups located on the surface of the electrode formed some sort of covalent bond with *glutamate* at a physiologically relevant temperature of 37 °C with a nominal voltage bias is very encouraging and builds a case for the effectiveness of GC as a *glutamate*-sensing electrode material. The presence of these bonds also points to the potential durability of this surface func-

tionalization. In a broader sense, for the detection of analytes with low detection limits, two critical components have to be addressed, namely the fast diffusion of these analytes in the medium and their subsequent adsorption on the surface of microelectrodes [69]. With regard to developing an understanding of the rate of *glutamate* molecules' diffusion to the surface of carbon electrodes, both experimental and simulation works are currently absent in the literature and, as a consequence, this research area remains unexplored. On the other hand, regarding the adsorption of *glutamate* on the surface of carbon microelectrodes, the presence of active functional groups in the microelectrodes that promote covalent bonds plays a significant role [48]. The demonstration of a strong covalent bond formation between GC's surface and *glutamate* reported here, therefore, offers strong evidence that GC microelectrodes promote good adsorption of *glutamate* on their surface; hence, this directly contributes to the literature of *glutamate* detection through carbon microelectrodes. Taken together, the outcomes reported here further support the effectiveness of GC microelectrodes for sensing *glutamate* at low detection limits.

With the presence of strong covalent bonds between the surface of the GC electrode and the functionalization enzyme established, our next task was to demonstrate the validity and effectiveness of the indirect voltametric detection of *glutamate* through its byproduct of  $H_2O_2$ . The evidence presented in this research indicates strong correlations between  $H_2O_2$  and *glutamate*, enabling the detection of a 10 nM concentration of *glutamate*, which is an important milestone. In the broader context of establishing the usefulness of GC for neurotransmitter detection, we had previously demonstrated excellent performance of GC with regard to the key issues of resistance to biofouling, stability of the microelectrodes, and selectivity of analytes [48]. Further, consistent with our previous work, the current peak amplitudes recorded here during FSCV were stable over the recording sessions with no significant drifting observed, once again demonstrating the electrochemical stability and reproducibility of the GC microelectrodes [48]. These excellent stability and anti-fouling properties are further aided by the hydrophilic nature of GC due to its defect-rich surfaces and reactive edges that consist of abundant dangling bonds [69]. In addition, while GC microelectrodes have demonstrated the capability for simultaneous and separated in vitro detection of the reduction in and oxidation peaks of *dopamine* and *serotonin*, we now have also carried out a new experiment to establish selectivity in the context of  $H_2O_2$  with *dopamine* and *serotonin* in this study (Supplementary Figure S4). The lower limit of detection (LOD) of the microelectrodes was also calculated through a regression analysis of the standard curves, where the calibration plot ( $n = 7$ ) followed a linear trend in the 10 nM–2  $\mu$ M range, as shown in Supplementary Figure S5. The theoretical lower detection limit (LOD), defined as three times the standard deviation of the noise, was estimated to be 1.51 and 1.71 nM for *glutamate* and  $H_2O_2$ , respectively [70]. These compare very well with the reported LOD of 1.11 and 1.29 nM for *dopamine* and *serotonin*, respectively, using GC microelectrodes [48].

Collectively, the results presented here on the in vitro detection of *glutamate* with the modified GC microelectrodes through a wide range of concentrations of the enzymatic *glutamate* conversion's byproduct are promising in extending the usefulness and compelling advantage of GC microelectrodes for the detection of non-electroactive neurotransmitters. In conclusion, the validation of the in vitro data presented through in vivo testing, the demonstration of the detection of other non-electroactive neurotransmitters such as *lactate*, and—more importantly—the simultaneous detection of electroactive and non-electroactive neurotransmitters on the same probe are a natural extension of this current work.

**Supplementary Materials:** The following supporting information can be downloaded at: <https://www.mdpi.com/article/10.3390/c10030068/s1>, Figure S1. Compression test plot for (a) force–time and (b) close-up stress–strain curve for 0.6% agarose hydrogel model; Figure S2. Tips before and after penetration tests; Figure S3. Reactions driving FSCV detection on *GluOx*-functionalized GC microelectrode; Figure S4. Experimenting for demonstrating selectivity of analytes using GC microelectrodes. In this experiment, we injected a mix of 40 nM of serotonin and 40 nM of  $H_2O_2$  and used GC microelectrode to selectively detect the distinct oxidation and reduction in serotonin along

with the distinct H<sub>2</sub>O<sub>2</sub> peaks. We repeated the same experiment for a mix of 100 nM of dopamine and 100 nM of H<sub>2</sub>O<sub>2</sub> where, again, distinct peaks of the two analytes were determined, as shown below; Figure S5. Lower limit of detection (LOD) of the microelectrodes was estimated to be 1.71 and 1.51 nM for H<sub>2</sub>O<sub>2</sub> and *glutamate*, respectively; Table S1. Active site amino acids of glutamate oxidase (GluOX); Table S2. Injection of *glutamate* and H<sub>2</sub>O<sub>2</sub> as a function of time with sufficient time provided in-between each step to allow for stabilization of FSCV data collection.

**Author Contributions:** S.L.G. fabricated the devices, implemented the microfabrication process, analyzed the results, and wrote the Materials and Methods and the Results sections of this paper; S.N. helped set up the molecular dynamic simulations; A.O. helped in microfabrication; J.B. helped with plots and analysis; O.N.C. helped with SEM imaging; R.M.-W. helped set up the molecular dynamic simulations; A.R. helped in microelectrode characterization; B.K.C. and A.G. helped in microfabrication; K.P.-G. helped with FTIR; J.L. helped with MATLAB plots; S.I.B. designed and carried out the mechanical characterizations; C.F. helped with the chemistry of *glutamate oxidase* and *glutamate* as they relate to MD modeling; S.S.K. reviewed the manuscript; S.K. formulated the concept, supervised the project, structured the outline of this paper, edited the manuscript, and wrote the Introduction and the Discussions and Conclusion sections of this paper. All authors have read and agreed to the published version of the manuscript.

**Funding:** This research is funded by the Center for Neurotechnology (CNT), a National Science Foundation Engineering Research Center (EEC-1028725) and NSF AccelNet: Broadening Carbon Ring program (Award no. 2301898). S.I.B. and S.S.K. acknowledge funding from the Independent Research Fund Denmark (Grant no. 8022-00215B).

**Data Availability Statement:** Data is available upon request.

**Conflicts of Interest:** The authors declare no conflict of interest.

## References

1. Si, B.; Song, E. Recent Advances in the Detection of Neurotransmitters. *Chemosensors* **2018**, *6*, 1. [[CrossRef](#)]
2. Puskarjov, M.; Seja, P.; E Heron, S.; Williams, T.C.; Ahmad, F.; Iona, X.; Oliver, K.L.; E Grinton, B.; Vutskits, L.; E Scheffer, I.; et al. A variant of KCC2 from patients with febrile seizures impairs neuronal Cl<sup>-</sup> extrusion and dendritic spine formation. *Embo Rep.* **2014**, *15*, 723–729. [[CrossRef](#)] [[PubMed](#)]
3. Lotharius, J.; Brundin, P. Pathogenesis of Parkinson's disease: Dopamine, vesicles and  $\alpha$ -synuclein. *Nat. Rev. Neurosci.* **2002**, *3*, 932–942. [[CrossRef](#)] [[PubMed](#)]
4. Gründer, G.; Cumming, P. Computational Neuroanatomy of Schizophrenia. *Neurobiol. Schizophr.* **2016**, *1*, 263–282. [[CrossRef](#)]
5. Wise, R.A. Dopamine, learning and motivation. *Nat. Rev. Neurosci.* **2004**, *5*, 483–494. [[CrossRef](#)] [[PubMed](#)]
6. Haber, S.N.; Knutson, B. The Reward Circuit: Linking Primate Anatomy and Human Imaging. *Neuropsychopharmacology* **2009**, *35*, 4–26. [[CrossRef](#)] [[PubMed](#)]
7. Ryczko, D.; Dubuc, R. Dopamine and the Brainstem Locomotor Networks: From Lamprey to Human. *Front. Neurosci.* **2017**, *11*, 295. [[CrossRef](#)] [[PubMed](#)]
8. Felger, J.C.; Treadway, M.T. Inflammation Effects on Motivation and Motor Activity: Role of Dopamine. *Neuropsychopharmacology* **2016**, *42*, 216–241. [[CrossRef](#)]
9. Pithadia, A. 5-Hydroxytryptamine Receptor Subtypes and their Modulators with Therapeutic Potentials. *J. Clin. Med. Res.* **2009**, *1*, 72–80. [[CrossRef](#)]
10. Maffei, M.E. 5-Hydroxytryptophan (5-HTP): Natural Occurrence, Analysis, Biosynthesis, Biotechnology, Physiology and Toxicology. *Int. J. Mol. Sci.* **2020**, *22*, 181. [[CrossRef](#)]
11. Franco, R.; Rivas-Santisteban, R.; Lillo, J.; Camps, J.; Navarro, G.; Reyes-Resina, I. 5-Hydroxytryptamine, Glutamate, and ATP: Much More Than Neurotransmitters. *Front. Cell Dev. Biol.* **2021**, *9*, 667815. [[CrossRef](#)] [[PubMed](#)]
12. Gründer, G.; Cumming, P. The Dopamine Hypothesis of Schizophrenia: Current Status. In *The Neurobiology of Schizophrenia*; Abel, T., Nickl-Jockschat, T., Eds.; Elsevier Academic Press: Amsterdam, The Netherlands, 2016; pp. 109–124. [[CrossRef](#)]
13. Fakhoury, M. Revisiting the Serotonin Hypothesis: Implications for Major Depressive Disorders. *Mol. Neurobiol.* **2015**, *53*, 2778–2786. [[CrossRef](#)] [[PubMed](#)]
14. Schloss, P.; Williams, D.C. The serotonin transporter: A primary target for antidepressant drugs. *J. Psychopharmacol.* **1998**, *12*, 115–121. [[CrossRef](#)] [[PubMed](#)]
15. Yohn, C.N.; Gergues, M.M.; Samuels, B.A. The role of 5-HT receptors in depression. *Mol. Brain* **2017**, *10*, 28. [[CrossRef](#)]
16. Celada, P.; Puig, M.V.; Artigas, F. Serotonin modulation of cortical neurons and networks. *Front. Integr. Neurosci.* **2013**, *7*, 25. [[CrossRef](#)] [[PubMed](#)]
17. Zhou, Y.; Danbolt, N.C. Glutamate as a neurotransmitter in the healthy brain. *J. Neural Transm.* **2014**, *121*, 799–817. [[CrossRef](#)] [[PubMed](#)]

18. Ramadan, S.; Lin, A.; Stanwell, P. Glutamate and glutamine: A review of in vivo MRS in the human brain. *NMR Biomed.* **2013**, *26*, 1630–1646. [[CrossRef](#)] [[PubMed](#)]
19. Barker-Haliski, M.; White, H.S. Glutamatergic Mechanisms Associated with Seizures and Epilepsy. *Cold Spring Harb. Perspect. Med.* **2015**, *5*, a022863. [[CrossRef](#)] [[PubMed](#)]
20. Statstrom, C.E.; Carmant, L. Seizures and Epilepsy: An Overview. In *Epilepsy: The Intersection of Neurosciences, Biology, Mathematics, Engineering, and Physics*; CRC Press: Boca Raton, FL, USA, 2016; pp. 65–77. [[CrossRef](#)]
21. Beghi, E. The Epidemiology of Epilepsy. *Neuroepidemiology* **2019**, *54*, 185–191. [[CrossRef](#)]
22. Furness, A.M.; Pal, R.; Michealis, E.K.; Lunte, C.E.; Lunte, S.M. Neurochemical investigation of multiple locally induced seizures using microdialysis sampling: Epilepsy effects on glutamate release. *Brain Res.* **2019**, *1722*, 146360. [[CrossRef](#)]
23. Lee, D.J.; Lozano, C.S.; Dallapiazza, R.F.; Lozano, A.M. Current and future directions of deep brain stimulation for neurological and psychiatric disorders. *J. Neurosurg.* **2019**, *131*, 333–342. [[CrossRef](#)] [[PubMed](#)]
24. Moran, S.P.; Maksymetz, J.; Conn, P.J. Targeting Muscarinic Acetylcholine Receptors for the Treatment of Psychiatric and Neurological Disorders. *Trends Pharmacol. Sci.* **2019**, *40*, 1006–1020. [[CrossRef](#)] [[PubMed](#)]
25. McCutcheon, R.A.; Marques, T.R.; Howes, O.D. Schizophrenia—An Overview. *JAMA Psychiatry* **2020**, *77*, 201–210. [[CrossRef](#)] [[PubMed](#)]
26. Poewe, W.; Seppi, K.; Tanner, C.M.; Halliday, G.M.; Brundin, P.; Volkmann, J.; Schrag, A.E.; Lang, A.E. Parkinson disease. *Nat. Rev. Dis. Primers* **2017**, *3*, 17013. [[CrossRef](#)] [[PubMed](#)]
27. Kandel, E.R.; Schwartz, J.H.; Jessell, T.M.; Siegelbaum, S.A.; Hudspeth, A.J.; Mack, S. (Eds.) *Principles of Neural Science*, 5th ed.; McGraw Hill: New York, NY, USA, 2014.
28. Ludwig, P.E.; Reddy, V.; Varacallo, M. *Neuroanatomy, Central Nervous System (CNS)*; StatPearls Publishing: Treasure Island, FL, USA, 2022.
29. Obien, M.E.J.; Deligkaris, K.; Bullmann, T.; Bakkum, D.J.; Frey, U. Revealing neuronal function through microelectrode array recordings. *Front. Neurosci.* **2015**, *8*, 423. [[CrossRef](#)] [[PubMed](#)]
30. Pereda, A.E. Electrical synapses and their functional interactions with chemical synapses. *Nat. Rev. Neurosci.* **2014**, *15*, 250–263. [[CrossRef](#)] [[PubMed](#)]
31. Bozorgzadeh, B.; Schuweiler, D.R.; Bobak, M.J.; Garris, P.A.; Mohseni, P. Neurochemostat: A Neural Interface SoC with Integrated Chemometrics for Closed-Loop Regulation of Brain Dopamine. *IEEE Trans. Biomed. Circuits Syst.* **2015**, *10*, 654–667. [[CrossRef](#)] [[PubMed](#)]
32. Grahn, P.J.; Mallory, G.W.; Khurram, O.U.; Berry, B.M.; Hachmann, J.T.; Bieber, A.J.; Bennet, K.E.; Min, H.-K.; Chang, S.-Y.; Lee, K.H.; et al. A neurochemical closed-loop controller for deep brain stimulation: Toward individualized smart neuromodulation therapies. *Front. Neurosci.* **2014**, *8*, 169. [[CrossRef](#)] [[PubMed](#)]
33. Bath, B.D.; Michael, D.J.; Trafton, B.J.; Joseph, J.D.; Runnels, P.L.; Wightman, R.M. Subsecond Adsorption and Desorption of Dopamine at Carbon-Fiber Microelectrodes. *Anal. Chem.* **2000**, *72*, 5994–6002. [[CrossRef](#)]
34. Kim, D.H.; Oh, Y.; Shin, H.; Park, C.; Blaha, C.D.; Bennet, K.E.; Kim, I.Y.; Lee, K.H.; Jang, D.P. Multi-waveform fast-scan cyclic voltammetry mapping of adsorption/desorption kinetics of biogenic amines and their metabolites. *Anal. Methods* **2018**, *10*, 2834–2843. [[CrossRef](#)]
35. Shadlaghani, A.; Farzaneh, M.; Kinser, D.; Reid, R.C. Direct Electrochemical Detection of Glutamate, Acetylcholine, Choline, and Adenosine Using Non-Enzymatic Electrodes. *Sensors* **2019**, *19*, 447. [[CrossRef](#)] [[PubMed](#)]
36. Xia, Y.; Li, G.; Zhu, Y.; He, Q.; Hu, C. Facile Preparation of Metal-Free Graphitic-Like Carbon Nitride/Graphene Oxide Composite for Simultaneous Determination of Uric Acid and Dopamine. *Microchem. J.* **2023**, *190*, 108726. [[CrossRef](#)]
37. Zhang, M.; Liao, C.; Yao, Y.; Liu, Z.; Gong, F.; Yan, F. High-Performance Dopamine Sensors Based on Whole-Graphene Solution-Gated Transistors. *Adv. Funct. Mater.* **2014**, *24*, 978–985. [[CrossRef](#)]
38. Okon, S.L.; Ronkainen, N.J. Enzyme-Based Electrochemical Glutamate Biosensors. In *Electrochemical Sensors Technology*; Rahman, M.M., Asiri, A.M., Eds.; IntechOpen: London, UK, 2017. [[CrossRef](#)]
39. Shin, M.; Wang, Y.; Borgus, J.R.; Venton, B.J. Electrochemistry at the Synapse. *Annu. Rev. Anal. Chem.* **2019**, *12*, 297–321. [[CrossRef](#)] [[PubMed](#)]
40. Kimble, L.C.; Twiddy, J.S.; Berger, J.M.; Forderhase, A.G.; McCarty, G.S.; Meitzen, J.; Sombers, L.A. Simultaneous, Real-Time Detection of Glutamate and Dopamine in Rat Striatum Using Fast-Scan Cyclic Voltammetry. *ACS Sens.* **2023**, *8*, 4091–4100. [[CrossRef](#)] [[PubMed](#)]
41. Swamy, B.E.K.; Venton, B.J. Carbon nanotube-modified microelectrodes for simultaneous detection of dopamine and serotonin in vivo. *Analyst* **2007**, *132*, 876–884. [[CrossRef](#)] [[PubMed](#)]
42. Manciu, F.S.; Oh, Y.; Barath, A.; Rusheen, A.E.; Kouzani, A.Z.; Hodges, D.; Guerrero, J.; Tomshine, J.; Lee, K.H.; Bennet, K.E. Analysis of Carbon-Based Microelectrodes for Neurochemical Sensing. *Materials* **2019**, *12*, 3186. [[CrossRef](#)] [[PubMed](#)]
43. Swinya, D.L.; Swinya, D.L.; Martín-Yerga, D.; Martín-Yerga, D.; Walker, M.; Walker, M.; Unwin, P.R.; Unwin, P.R. Surface Nanostructure Effects on Dopamine Adsorption and Electrochemistry on Glassy Carbon Electrodes. *J. Phys. Chem. C* **2022**, *126*, 13399–13408. [[CrossRef](#)] [[PubMed](#)]
44. Khoshnevisan, K.; Honarvarfard, E.; Torabi, F.; Maleki, H.; Baharifar, H.; Faridbod, F.; Larijani, B.; Khorramizadeh, M.R. Electrochemical detection of serotonin: A new approach. *Clin. Chim. Acta* **2019**, *501*, 112–119. [[CrossRef](#)]

45. Mendoza, A.; Asrat, T.; Liu, F.; Wonnenberg, P.; Zestos, A.G. Carbon Nanotube Yarn Microelectrodes Promote High Temporal Measurements of Serotonin Using Fast Scan Cyclic Voltammetry. *Sensors* **2020**, *20*, 1173. [[CrossRef](#)]
46. Abdalla, A.; Atcherley, C.W.; Pathirathna, P.; Samaranyake, S.; Qiang, B.; Peña, E.; Morgan, S.L.; Heien, M.L.; Hashemi, P. In Vivo Ambient Serotonin Measurements at Carbon-Fiber Microelectrodes. *Anal. Chem.* **2017**, *89*, 9703–9711. [[CrossRef](#)] [[PubMed](#)]
47. Castagnola, E.; Vahidi, N.W.; Nimbalkar, S.; Rudraraju, S.; Thielk, M.; Zucchini, E.; Cea, C.; Carli, S.; Gentner, T.Q.; Ricci, D.; et al. In Vivo Dopamine Detection and Single Unit Recordings Using Intracortical Glassy Carbon Microelectrode Arrays. *MRS Adv.* **2018**, *3*, 1629–1634. [[CrossRef](#)] [[PubMed](#)]
48. Castagnola, E.; Thongpang, S.; Hirabayashi, M.; Nava, G.; Nimbalkar, S.; Nguyen, T.; Lara, S.; Oyawale, A.; Bunnell, J.; Moritz, C.; et al. Glassy carbon microelectrode arrays enable voltage-peak separated simultaneous detection of dopamine and serotonin using fast scan cyclic voltammetry. *Analyst* **2021**, *146*, 3955–3970. [[CrossRef](#)]
49. Qin, S.; Van der Zeyden, M.; Oldenzel, W.H.; Cremers, T.I.; Westerink, B.H. Microsensors for in vivo Measurement of Glutamate in Brain Tissue. *Sensors* **2008**, *8*, 6860–6884. [[CrossRef](#)] [[PubMed](#)]
50. van der Zeyden, M.; Oldenzel, W.H.; Rea, K.; Cremers, T.I.; Westerink, B.H. Microdialysis of GABA and glutamate: Analysis, interpretation and comparison with microsensors. *Pharmacol. Biochem. Behav.* **2008**, *90*, 135–147. [[CrossRef](#)] [[PubMed](#)]
51. Meng, L.; Wu, P.; Chen, G.; Cai, C.; Sun, Y.; Yuan, Z. Low potential detection of glutamate based on the electrocatalytic oxidation of NADH at thionine/single-walled carbon nanotubes composite modified electrode. *Biosens. Bioelectron.* **2009**, *24*, 1751–1756. [[CrossRef](#)]
52. Vomero, M.; Castagnola, E.; Ciarpella, F.; Maggolini, E.; Goshi, N.; Zucchini, E.; Carli, S.; Fadiga, L.; Kassegne, S.; Ricci, D. Highly Stable Glassy Carbon Interfaces for Long-Term Neural Stimulation and Low-Noise Recording of Brain Activity. *Sci. Rep.* **2017**, *7*, 40332. [[CrossRef](#)] [[PubMed](#)]
53. Vomero, M.; van Niekerk, P.; Nguyen, V.; Gong, N.; Hirabayashi, M.; Cinopri, A.; Logan, K.; Moghadasi, A.; Varma, P.; Kassegne, S. A novel pattern transfer technique for mounting glassy carbon microelectrodes on polymeric flexible substrates. *J. Micromech. Microeng.* **2016**, *26*, 025018. [[CrossRef](#)]
54. Nimbalkar, S.; Castagnola, E.; Balasubramani, A.; Scarpellini, A.; Samejima, S.; Khorasani, A.; Boissenin, A.; Thongpang, S.; Moritz, C.; Kassegne, S. Ultra-Capacitive Carbon Neural Probe Allows Simultaneous Long-Term Electrical Stimulations and High-Resolution Neurotransmitter Detection. *Sci. Rep.* **2018**, *8*, 6958. [[CrossRef](#)]
55. Bisgaard, S.I.; Nguyen, L.Q.; Bøgh, K.L.; Keller, S.S. Dermal tissue penetration of in-plane silicon microneedles evaluated in skin-simulating hydrogel, rat skin and porcine skin. *Mater. Sci. Eng. C* **2023**, *155*, 213659. [[CrossRef](#)]
56. Pomfret, R.; Miranpuri, G.; Sillay, K. The Substitute Brain and the Potential of the Gel Model. *Ann. Neurosci.* **2013**, *20*, 118–122. [[CrossRef](#)] [[PubMed](#)]
57. Budday, S.; Ovaert, T.C.; Holzapfel, G.A.; Steinmann, P.; Kuhl, E. Fifty Shades of Brain: A Review on the Mechanical Testing and Modeling of Brain Tissue. *Arch. Comput. Methods Eng.* **2020**, *27*, 1187–1230. [[CrossRef](#)]
58. Singh, D.; Boakye-Yiadom, S.; Cronin, D. Comparison of porcine brain mechanical properties to potential tissue simulant materials in quasi-static and sinusoidal compression. *J. Biomech.* **2019**, *92*, 84–91. [[CrossRef](#)] [[PubMed](#)]
59. Van Duin, A.C.T.; Dasgupta, S.; Lorant, F.; Goddard, W.A. ReaxFF: A Reactive Force Field for Hydrocarbons. *J. Phys. Chem. A* **2001**, *105*, 9396–9409. [[CrossRef](#)]
60. Montgomery-Walsh, R.; Nimbalkar, S.; Bunnell, J.; Galindo, S.L.; Kassegne, S. Molecular dynamics simulation of evolution of nanostructures and functional groups in glassy carbon under pyrolysis. *Carbon* **2021**, *184*, 627–640. [[CrossRef](#)]
61. Senftle, T.P.; Hong, S.; Islam, M.M.; Kylasa, S.B.; Zheng, Y.; Shin, Y.K.; Junkermeier, C.; Engel-Herbert, R.; Janik, M.J.; Aktulga, H.M.; et al. The ReaxFF Reactive Force-Field: Development, Applications and Future Directions. *NPI Comput. Mater.* **2016**, *2*, 15011. [[CrossRef](#)]
62. Russo, M.F., Jr.; van Duin, A.C.T. Atomistic-Scale Simulations of Chemical Reactions: Bridging from Quantum Chemistry to Engineering. *Nucl. Instrum. Methods Phys. Res. B* **2011**, *269*, 1549–1554. [[CrossRef](#)]
63. Nandiyanto, A.B.D.; Oktiani, R.; Ragadhita, R. How to Read and Interpret FTIR Spectroscopy of Organic Material. *Indones. J. Sci. Technol.* **2019**, *4*, 97–118. [[CrossRef](#)]
64. Mureşan-Pop, M.; Kacsó, I.; Filip, X.; Vanea, E.; Borodi, G.; Leopold, N.; Bratu, I.; Simon, S. Spectroscopic and Physical-Chemical Characterization of Ambazone-Glutamate Salt. *Spectroscopy* **2011**, *26*, 115–128. [[CrossRef](#)]
65. Jayaraman, V.; Keeseey, R.; Madden, D.R. Ligand–Protein Interactions in the Glutamate Receptor. *Biochemistry* **2000**, *39*, 8693–8697. [[CrossRef](#)]
66. Batra, B.; Pundir, C. An amperometric glutamate biosensor based on immobilization of glutamate oxidase onto carboxylated multiwalled carbon nanotubes/gold nanoparticles/chitosan composite film modified Au electrode. *Biosens. Bioelectron.* **2013**, *47*, 496–501. [[CrossRef](#)] [[PubMed](#)]
67. Tonel, M.Z.; González-Durruthy, M.; Zanella, I.; Fagan, S.B. Interactions of Graphene Derivatives with Glutamate-Neurotransmitter: A Parallel First Principles—Docking Investigation. *J. Mol. Graph. Model.* **2019**, *88*, 121–127. [[CrossRef](#)] [[PubMed](#)]
68. Sanford, A.L.; Morton, S.W.; Whitehouse, K.L.; Oara, H.M.; Lugo-Morales, L.Z.; Roberts, J.G.; Sombers, L.A. Voltammetric Detection of Hydrogen Peroxide at Carbon Fiber Microelectrodes. *Anal. Chem.* **2010**, *82*, 5205–5210. [[CrossRef](#)] [[PubMed](#)]



- 
69. Puthongkham, P.; Venton, B.J. Recent advances in fast-scan cyclic voltammetry. *Analyst* **2019**, *145*, 1087–1102. [[CrossRef](#)]
  70. Schmidt, A.C.; Wang, X.; Zhu, Y.; Sombers, L.A. Carbon nanotube yarn electrodes for enhanced detection of neurotransmitter dynamics in live brain tissue. *ACS Nano* **2013**, *7*, 7864–7873. [[CrossRef](#)]

**Disclaimer/Publisher's Note:** The statements, opinions and data contained in all publications are solely those of the individual author(s) and contributor(s) and not of MDPI and/or the editor(s). MDPI and/or the editor(s) disclaim responsibility for any injury to people or property resulting from any ideas, methods, instructions or products referred to in the content.